Monitoring Afatinib Treatment in HER2-Positive Gastric Cancer with ^{18}F-FDG and ^{89}Zr-Trastuzumab PET

Yelena Y. Janjigian*[1], Nerissa Viola-Villegas*[2], Jason P. Holland[2], Vadim Divilov[2], Sean D. Carlin[2], Erica M. Gomes-DaGama[3], Gabriela Chiosis[3], Gregory Carbonetti[4], Elisa de Stanchina[4], and Jason S. Lewis[2,3]

[1]*Gastrointestinal Oncology Service, Department of Medicine, Memorial Sloan-Kettering Cancer Center, New York, NY;* [2]*Radiochemistry and Imaging Sciences Service, Department of Radiology, Memorial Sloan-Kettering Cancer Center, New York, NY;* [3]*Molecular Pharmacology and Chemistry Program, Memorial Sloan-Kettering Cancer Center, New York, NY; and* [4]*Antitumor Assessment Core Facility, Memorial Sloan-Kettering Cancer Center, New York, NY.*

We evaluated the ability of the PET imaging agent ^{89}Zr-trastuzumab to delineate HER2-positive gastric cancer and to monitor the pharmacodynamic effects of the epidermal growth factor receptor (EGFR)/human epidermal growth factor receptor 2 (HER2) tyrosine kinase inhibitor afatinib. **Methods:** Using ^{89}Zr-trastuzumab, ^{18}F-FDG, or 3′-deoxy-3′-^{18}F-fluorothymidine (^{18}F-FLT PET), we imaged HER2-positive NCI-N87 and HER2-negative MKN74 gastric cancer xenografts in mice. Next, we examined the pharmacodynamic effects of afatinib in NCI-N87 xenografts using ^{89}Zr-trastuzumab and ^{18}F-FDG PET and comparing imaging results to changes in tumor size and in protein expression as monitored by Western blot and histologic studies. **Results:** Although ^{18}F-FDG uptake in NCI-N87 tumors did not change, a decrease in ^{89}Zr-trastuzumab uptake was observed in the afatinib-treated versus control groups (3.0 ± 0.0 percentage injected dose per gram (%ID/g) vs. 21.0 ± 3.4 %ID/g, respectively; $P < 0.05$). ^{89}Zr-trastuzumab PET results corresponded with tumor reduction, apoptosis, and downregulation of HER2 observed on treatment with afatinib. Downregulation of total HER2, phosphorylated (p)-HER2, and p-EGFR occurred within 24 h of the first dose of afatinib, with a sustained effect over 21 d of treatment. **Conclusion:** Afatinib demonstrated antitumor activity in HER2-positive gastric cancer in vivo. ^{89}Zr-trastuzumab PET specifically delineated HER2-positive gastric cancer and can be used to measure the pharmacodynamic effects of afatinib.

Key Words: gastric cancer; afatinib; HER2; ^{89}Zr-trastuzumab; ^{18}F-FDG

J Nucl Med 2013; 54:936–943
DOI: 10.2967/jnumed.112.110239

Each year worldwide, approximately 200,000 people are diagnosed with human epidermal growth factor receptor 2 (HER2)–positive esophagogastric cancer (*1–3*). A randomized phase III trial study for patients with this disease showed improved response and survival when trastuzumab (HER2-directed monoclonal antibody) was added to chemotherapy (*4*), and the U.S. Food and Drug Administration and European Union have approved trastuzumab for patients with HER2-positive esophagogastric cancer.

The *HER2* oncogene (also referred to as *HER2/neu* or *erbB-2*) on chromosome 17q21 encodes a 185-kDa transmembrane tyrosine kinase receptor that belongs to the erbB family comprising epidermal growth factor receptor (EGFR)/HER1, HER2, HER3, and HER4. HER2 activation plays a pivotal role in cell proliferation and survival, largely mediated through the RAS–MAPK pathway, and it inhibits cell death through the phosphatidylinositol 3′-kinase–AKT–mammalian target of rapamycin (mTOR) pathway (*5*). Although anti-HER2 therapy with trastuzumab has shown efficacy in HER2-positive esophagogastric cancer (*4*), possible limitations to this approach include incomplete blockade of EGFR and HER2 kinase activity and coincident activation of other members of the erbB family.

Afatinib (BIBW 2992)—a highly selective, irreversible inhibitor of the erbB family of tyrosine kinase receptors EGFR, HER2, and HER4—is currently in phase II–III studies in lung (*6*), head and neck (*7,8*), and breast cancers (*9*). Afatinib monotherapy in HER2-driven tumors has decreased tumor size in phase II studies of HER2-amplified breast cancer (*10*) and HER2 mutant lung cancer (*11*). Clinical efficacy of afatinib in patients with esophagogastric cancer has not yet been explored. We hypothesized that noninvasive imaging of HER2 might facilitate anti-HER2 therapies for esophagogastric cancer.

In patients with locally advanced esophagogastric adenocarcinoma, early metabolic response defined by ^{18}F-FDG PET during preoperative chemotherapy predicts histopathologic response and survival (*12–14*). These findings provide an important step toward tailoring treatment to tumor biology. However, the ability of trastuzumab to provide site-directed targeting of HER2-positive tumors cannot be achieved by ^{18}F-FDG. Moreover, approximately 30% of gastric cancers cannot be visualized with sufficient con-

Received Jun. 19, 2012; revision accepted Nov. 27, 2012.
For correspondence or reprints contact either of the following:
Jason S. Lewis, Radiochemistry and Imaging Sciences Service, Memorial Sloan-Kettering Cancer Center, 415 E. 68th St., P.O. Box 394, New York, NY 10065.
E-mail: lewisj2@mskcc.org
Yelena Y. Janjigian, Gastrointestinal Oncology Service, Memorial Sloan-Kettering Cancer Center, 300 E. 66th St., New York, NY 10065.
E-mail: janjigiy@mskcc.org
*Contributed equally to this work.
Published online Apr. 11, 2013.

trast for quantification on ^{18}F-FDG PET (*15*). Previous methods have investigated the use of trastuzumab labeled with radionuclides including ^{64}Cu- and ^{68}Ga-labeled F(ab′)$_2$ fragments (*16–18*). The images obtained using these agents show relatively poor tumor–to–background tissue contrast due to the short radioactive half-life ($t_{1/2}$) (^{64}Cu), which fails to match optimum biodistribution profiles or the small molecule size (^{68}Ga-F(ab′)$_2$) of these molecules. However, the physical decay properties of the positron emitter ^{89}Zr ($t_{1/2}$ = 78.4 h) are ideal for PET imaging with larger vectors such as full antibodies and lead to image resolution comparable to that obtained with ^{18}F-FDG (*19,20*).

In this study, we examined the utility of ^{89}Zr-trastuzumab PET analysis as a biomarker to identify HER2-positive esophagogastric cancer and evaluated the biologic effects of afatinib in human HER2-positive gastric xenograft models. Validation of this hypothesis will mean a decrease in tumor uptake of ^{89}Zr-trastuzumab as a consequence of EGFR/HER2 inhibition.

MATERIALS AND METHODS

All chemicals were purchased from Sigma-Aldrich, unless otherwise stated. Radioactivity was measured using a CRC-55tR dose calibrator (Capintec) with a calibration factor of 465 for ^{89}Zr and an Automatic Wizard^2 γ-counter (Perkin Elmer) set to decay-correct at the start of the assay. Purity and radiochemical yields were determined using a Bioscan AR2000 (Bioscan Inc.) chromatograph with Win-Scan radio–thin-layer chromatography software (version 3.13; Bioscan Inc.).

Afatinib Treatment in NCI-N87 HER2-Positive Xenograft

Gastric cancer cell lines NCI-N87 (HER2-positive) and MKN74 (HER2-negative) were obtained from the American Type Culture Collection and cultured in RPMI-1640 medium supplemented with 10% fetal calf serum (Omega Scientific) and 100 units/mL of both penicillin and streptomycin.

All animal experiments were performed in accordance with guidelines set by Memorial Sloan-Kettering Cancer Center Animal Care and Use Committee and Research Animal Resource Center.

Eight-week-old athymic *nu/nu* female mice (Harlan) were subcutaneously implanted on the left shoulder with 5×10^6 NCI-N87 cells along with Matrigel (BD Biosciences). When tumors reached approximately 150 mm^3, 10 animals per group were randomized to receive vehicle alone, oral afatinib (25 or 50 mg/kg daily; Boehringer Ingelheim, Inc.), trastuzumab (20 mg/kg once a week, intravenously; Genentech/Roche), or a combination of afatinib and trastuzumab over 21 d. Mice were observed daily throughout the treatment period for signs of morbidity or mortality. Tumors were measured twice weekly using calipers, and volume was calculated using the formula length × width^2 × 0.52. Tumor samples were collected within 8 h of the last treatment and preserved in 4% paraformaldehyde or flash-frozen until further use.

Western Blotting and Immunohistochemistry

Tumors were homogenized in buffer containing 2% sodium dodecyl sulfate (SDS), 50 mM Tris (pH 7.4), and 10% glycerol supplemented with protease and phosphatase inhibitor cocktail (Roche). The lysate was sonicated, boiled for 5 min, and centrifuged at 14,000 rpm, 20 min, 4°C, and protein concentrations of the lysate were determined using the BCA kit (Pierce) according to the manufacturer's instructions. Protein lysates (50–100 μg) were electrophoretically resolved by SDS/polyacrylamide gel electrophoresis, transferred to nitrocellulose membrane, and probed with the indicated primary antibodies: p-EGFR (Tyr 1173; Cell Signaling Technology), Total EGFR (D38B1; Cell Signaling Technology), Total c-erb-2/Her2/neu Ab15 clone 3B5 (Neomarker), p-Her3 (Tyr1289; Cell Signaling Technology), and total AKT (Cell Signaling Technology). Signals were detected with Western blotting detection reagents (GE Healthcare). All antibodies were diluted 1:500. Total HER2 expression at baseline and after afatinib treatment was assessed by immunohistochemistry (Dako).

Trastuzumab Conjugation and ^{89}Zr Labeling

Conjugation of trastuzumab with ensuing labeling of ^{89}Zr was performed according to previously published literature (*21*). Briefly, desferrioxamine was attached to trastuzumab via a succinic anhydride linker at a ratio of 10:1 (desferrioxamine: trastuzumab). The trastuzumab–desferrioxamine conjugate was then purified using a PD10 desalting column (GE Healthcare Lifesciences, U.K.).

^{89}Zr ($t_{1/2}$ = 78.4 h) was produced as reported previously (*19*). Radiolabeling reactions were performed according to previously reported methods (*20,21*). In summary, ^{89}Zr oxalate (~37 MBq) solution (pH ~7.0–7.2) was added to trastuzumab–desferrioxamine (300–350 μg). The reaction was incubated at room temperature for 1–1.5 h before purification. The purified labeled product was obtained via use of a PD10 desalting column or size-exclusion spin column centrifugation (molecular weight cut-off, 30 kDa; Amicon Ultra-4 [Millipore]). Radiochemical yields and purity were determined via radio–instant thin-layer chromatography. All radiolabeled antibodies were determined to have greater than 95% radiochemical and chemical purity before use. The number of desferrioxamine ligands conjugated to trastuzumab was determined via radiometric isotopic dilution experiments described previously (*22,23*).

The labeled trastuzumab was evaluated for its ability to bind to the HER2-positive NCI-N87 cell line using the protocol specified by Lindmo et al. (*24*). The immunoreactivity was determined via linear extrapolation of the percentage bound labeled antibody to an infinite antigen excess.

Small-Animal PET Imaging and Biodistribution Studies

Small-animal PET studies were conducted using microPET-R4 and Focus 120 scanners (Concorde Microsystems) on dual–tumor-bearing mice (n = 3–4) with NCI-N87 and MKN74 cells implanted subcutaneously on the left and right shoulders, respectively. Quantification was performed using ASIPro VM software (Concorde Microsystems). Three-dimensional regions of interest (ROIs) were manually drawn on the tumor site to obtain the uptake of the tracer as the mean percentage injected dose per gram (%ID/g). ^{18}F-FDG (7.4–9.25 MBq) and 3′-deoxy-3′-^{18}F-fluorothymidine (^{18}F-FLT PET) (7.4–9.25 MBq) were injected in a lateral tail vein; images were recorded 1 h after injection. ^{89}Zr-trastuzumab (8.14–10.18 MBq, 80–100 μg of protein) was administered to the same group of mice 24 h later, with images recorded between 4 and 96 h after injection.

Mice bearing NCI-N87 xenografts (n = 3–4/group) treated with either vehicle or afatinib (50 mg/kg) daily over 7–21 d were imaged with ^{18}F-FDG and ^{89}Zr-trastuzumab (Supplemental Fig. 4A; supplemental materials are available online only at http://jnm.snmjournals.org),

and PET imaging results were compared with tumor size, Western blot, and histology data.

In biodistribution experiments, ^{89}Zr-trastuzumab (0.37–0.555 MBq, 4–5 μg) was administered intravenously at 0 h. Untreated animals were euthanized at 24, 48, 96, and 144 h after injection (n = 3–5/group), and 12 organs (including the tumor) were counted for activity accumulation. A blocking study at 48 h was performed with a coinjection of a 100-μg excess of trastuzumab to demonstrate the uptake mechanism of the tracer. In biodistribution studies of mice treated with afatinib over 7, 14, and 21 d (n = 3–4/group), ^{89}Zr-trastuzumab was administered 24 h after the last day of treatment. The mice were euthanized a day later. Count data were background- and decay-corrected. Tissue uptake, measured in units of percentage injected dose per gram (%ID/g) for each sample, was calculated against the decay-corrected total net activity injected and normalized for tissue weight.

Digital Autoradiography and Microscopy

Digital autoradiography images were obtained as previously described (*25*), with minor modifications. Tumors were excised and flash-frozen, and 10-μm frozen sections were cut. Sections were then exposed to a phosphor plate for 24 h and subsequently read out at a 50-μm resolution using a BAS-1800II Bio-Imaging Analyzer (FujiFilm Medical Systems). The same sections were then stained with hematoxylin and eosin and imaged using a BX-60 microscope equipped with a CC12 Soft Imaging Systems camera (Olympus America). Images were registered manually using Adobe Photoshop software (version CS5; Adobe Systems).

Sequential sections were fixed in 4% paraformaldehyde and stained for HER2, the nuclear antigen Ki-67, and cleaved caspase 3. Staining was performed using a Discovery XT processor (Ventana Medical Systems). Rabbit polyclonal anti-Ki-67 (0.4 μg/mL; catalog no. VP-K451 [Vector Laboratories]) or anti-cleaved caspase 3 (Asp175) (0.1 μg/mL; catalog no. 9661 L [Cell Signaling]) was used after blocking, followed by biotinylated goat antirabbit IgG (catalog no. PK6101; Vector Laboratories) at a 1:200 dilution and detection with a DABMAP kit (Ventana Medical Systems) according to the manufacturer's instructions.

Quantitative data were expressed as mean ± SD. Statistical analysis was performed using a 1-way ANOVA test, followed by a Dunnett multiple-comparisons test. A P value of less than 0.05 was considered statistically significant.

RESULTS

Sensitivity of Afatinib

The efficacy of afatinib, trastuzumab, and the combination of afatinib and trastuzumab was examined in an NCI-N87 xenograft model; through fluorescence in situ hybridization and protein overexpression (immunohistochemistry), it was demonstrated that this model harbored HER2 gene amplification (Supplemental Figs. 1 and 2A). Although these tumors were relatively refractory to trastuzumab, afatinib monotherapy led to dramatic tumor volume regression within 4 d and near-complete tumor resolution after 21 d of treatment (Fig. 1A). We anticipated that together these agents would shrink tumors as was previously demonstrated with the combination of afatinib and cetuximab (a monoclonal antibody directed against EGFR) in an EGFR-driven lung cancer model harboring the T790 M mutation (*26*).The response with afatinib single-agent therapy in the NCI-N87 HER2-amplified model was so robust that the addition of trastuzumab to afatinib did not affect the overall potency of the treatment. Within 24–48 h, afatinib treatment correlated with downregulation of total HER2,

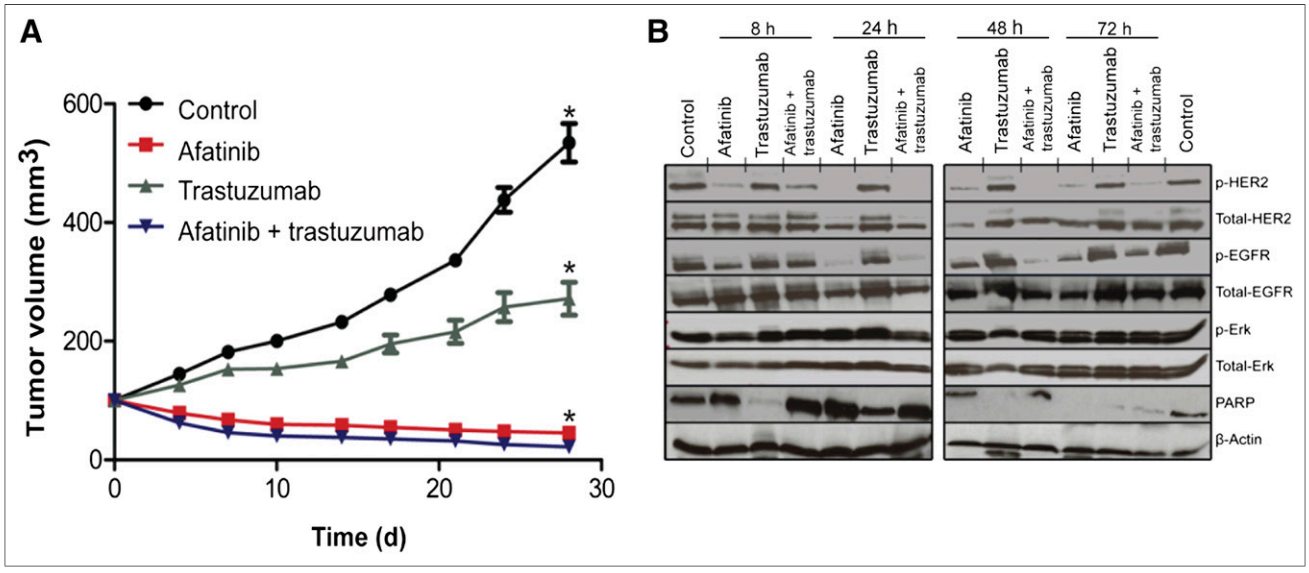

FIGURE 1. Effects of afatinib therapy in HER2-positive gastric cancer NCI-N87 xenograft. (A) Athymic nude mice bearing NCI-N87 tumors were treated (10 mice per group) with vehicle alone (intraperitoneally daily), afatinib (25 mg/kg orally daily), trastuzumab (20 mg/kg intravenously once a week), and combination of afatinib (25 mg/kg orally daily) with trastuzumab (20 mg/kg intravenously once a week). Tumor volume was measured twice a week after onset of treatment. (B) Western blot analyses of tumors harvested from HER2-positive NCI-N87 xenografts treated with afatinib (25 mg/kg) orally × 1 dose, specimen collected at 8, 24, 48, and 72 h after a single dose of afatinib. *$P < 0.05$, for afatinib vs. vehicle or trastuzumab alone.

p-HER2, p-EGFR, and induction of apoptosis as evidenced by cleavage of poly (ADP-ribose) polymerase in HER2-positive NCI-N87 xenografts (Fig.1B). Similarly, a decrease in total HER2 expression from baseline immunohistochemistry 3+ to immunohistochemistry 0/1+ was noted by immunohistochemical analysis of NCI-N87 tumors (24 h after a single dose of afatinib [25 mg/kg], with recovery of the signal [HER2 immunohistochemistry 2+] 24 h later) (Supplemental Figs. 2A–2C).

Radiochemistry and Characterization of ^{89}Zr-Trastuzumab

Conjugation of trastuzumab to desferrioxamine was achieved via an *N*-succinimidyl linkage with a monoclonal antibody:desferrioxamine ratio of approximately 1:4 as reported previously (*19,20*). Efficient labeling of trastuzumab with ^{89}Zr proceeded with high radiochemical yields of more than 70% and purities of more than 99%. The specific activity was determined to be approximately 105.5 ± 1.9 MBq/mg (2.82 ± 0.05 mCi/mg). The radiolabeled trastuzumab retained its immunoreactivity for HER2 by approximately 86.4 ± 0.44%.

Specificity of ^{89}Zr-Trastuzumab for HER2-Positive Gastric Tumor Through PET and Biodistribution

PET imaging with ^{89}Zr-trastuzumab proved highly specific for HER2-positive gastric tumors, whereas ^{18}F-FDG and ^{18}F-FLT PET were unable to differentiate HER2-positive from HER2-negative tumors. In vivo small-animal imaging with ^{18}F-FDG and ^{18}F-FLT, followed by sequential imaging with ^{89}Zr-trastuzumab on mice bearing NCI-N87 HER2-positive and MKN74 HER2-negative xenografts, showed excellent tumor accumulation of ^{89}Zr-trastuzumab for the HER2-amplified lesion. HER2-positive tumors were strongly PET-avid for ^{89}Zr-trastuzumab (Fig. 2), whereas HER2-negative tumors showed minimal ^{89}Zr-trastuzumab uptake. ROIs drawn from sequential ^{89}Zr-trastuzumab PET images of HER2-positive tumors display an uptake of 9.1 ± 2.1 % ID/g at 4 h after injection, with radiotracer accumulation doubled and peaked at 24 h and tumor-associated radioactivity retained for over 96 h after injection (18.1 ± 2.0 %ID/g, Supplemental Fig. 3A). In contrast, the HER2-negative tumor displayed 6.7 ± 0.8 %ID/g uptake at 24 h and remained at this level throughout the time course. The observed tracer binding seen on ROIs from the HER2-negative xenograft is nonspecific and may be attributed to permeation and enhanced retention of the tracer through the leaky vasculature of the tumor (Supplemental Fig. 3A) (*27*). In vivo biodistribution data showed a strong correlation with data from PET imaging with ^{89}Zr-trastuzumab (Supplemental Fig. 3B), demonstrating high and specific uptake in HER2-positive tumors. At 24 h after injection, 21.9 ± 3.7 %ID/g tumor accumulation was observed. Tumor-associated radioactivity was retained over 48 h (24.5 ± 7.5 %ID/g), 96 h (34.4 ± 9.0 %ID/g), and 144 h (36.6 ± 10.1 %ID/g). Coadministration of a 100-μg trastuzumab blocking dose with the radiotracer displayed a 2-fold decrease in tumor uptake (12.2 ± 2.2 %ID/g) at 48 h after injection. In contrast, both HER2-positive and HER2-negative tumors were PET-avid when imaged with ^{18}F-FDG (3.1 ± 0.5 %ID/g for the HER2-positive and 3.2 ± 0.7 %ID/g for the HER2-negative xenografts) and ^{18}F-FLT (8.0 ± 2.9 %ID/g for the HER2-positive and 8.7 ± 3.0 %ID/g for the HER2-negative tumors). We found no correlative agreement between the HER2 status of these tumors and ^{18}F-FDG and ^{18}F-FLT PET (Fig. 2).

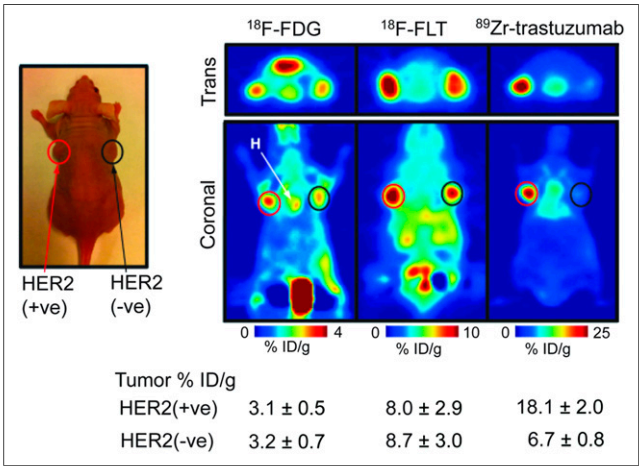

FIGURE 2. Specificity of ^{89}Zr-trastuzumab for HER2-positive tumors. Coronal ^{89}Zr-trastuzumab, ^{18}F-FDG, and ^{18}F-FLT PET images of athymic nude mice bearing subcutaneous HER2-positive NCI-N87(left) and HER2-negative MKN-74 (right) are shown. ROIs (%ID/g) for ^{89}Zr-trastuzumab, ^{18}F-FDG, and ^{18}F-FLT are indicated. +ve = positive; -ve = negative.

Monitoring of Afatinib Therapy

^{89}Zr-trastuzumab PET uptake decreased with afatinib therapy in HER2-positive gastric cancer. To monitor variations in ^{89}Zr-trastuzumab and ^{18}F-FDG uptake after treatment, NCI-N87 xenograft–bearing mice were treated with either vehicle or afatinib daily for 21 consecutive days and monitored by PET imaging once every 7 d (Fig. 3A). The uptake of ^{89}Zr-trastuzumab in tumors and normal organs was also examined with biodistribution experiments at days 7 and 21 (Supplemental Table 1). ^{89}Zr-trastuzumab demonstrated tumor specificity with low uptake in normal organs such as the liver, stomach, and intestines, providing a high tumor–to–normal tissue contrast ratio.

Baseline ^{89}Zr-trastuzumab tumor uptake from PET images was established at 14.4 ± 1.9 %ID/g. Within 7 d of afatinib treatment, we observed a 4-fold reduction in ^{89}Zr-trastuzumab tumor uptake (3.0 ± 0.5 %ID/g, $P < 0.001$) (Fig. 3B), whereas ^{18}F-FDG uptake remained constant. Figure 4A presents the quantitative ROI data drawn from both ^{89}Zr-trastuzumab and ^{18}F-FDG PET images and measured tumor weights of mice receiving therapy. Although ^{18}F-FDG uptake did not change significantly over time (Fig. 4A), ^{89}Zr-trastuzumab tumor uptake decreased,

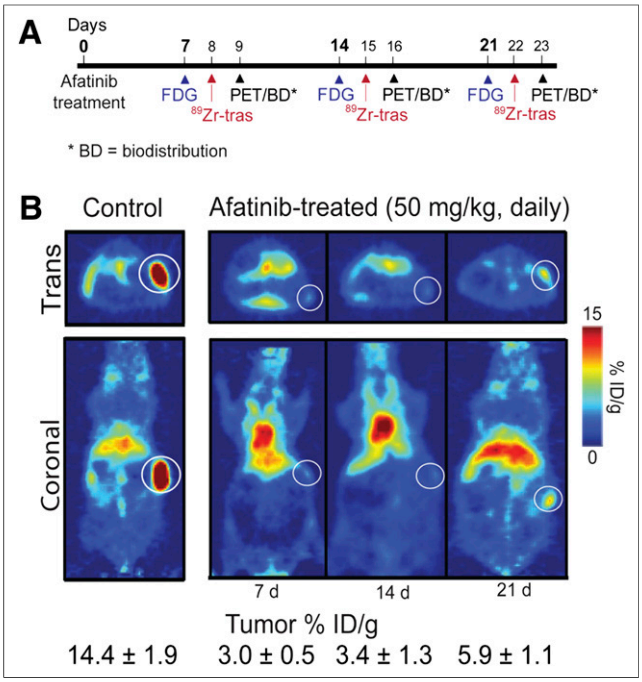

FIGURE 3. Effects of afatinib therapy in HER2-positive xenograft models. (A) Timeline of imaging and treatment experiments. (B) Coronal ^{89}Zr-trastuzumab PET images of control (left) and afatinib (right)-treated mice bearing subcutaneous HER2-positive NCI-N87 tumors. Trans = transaxial; tras = trastuzumab.

especially over the first 14 d of treatment, mirroring reduction in tumor weight and decrease in total HER2 as measured by immunoblot and immunohistochemistry.

In biodistribution studies (Supplemental Fig. 4), a decrease in ^{89}Zr-trastuzumab uptake was observed in HER2-positive tumors after 7 d of treatment with afatinib (50 mg/kg), compared with the control group (3.0 ± 0.5 %ID/g vs. 21.0 ± 3.4 %ID/g; $P < 0.01$). Daily treatment over the 21 d reduced tumor size and uptake to 5.9 ± 4.7 %ID/g ($P < 0.01$, Fig. 4A). Baseline ^{89}Zr-trastuzumab biodistribution was highest in the tumor (21.0 ± 3.4 %ID/g), compared with normal tissue (e.g., stomach, 0.5 ± 0.1 %ID/g). In HER2-positive tumors, decreased ^{89}Zr-trastuzumab uptake was observed with afatinib therapy, whereas no changes in ^{89}Zr-trastuzumab biodistribution were observed in normal tissues after afatinib (full biodistribution data are presented in Supplemental Table 1). ^{89}Zr-trastuzumab PET results corresponded with tumor size reduction and downregulation of total HER2, p-HER2, total EGFR, and p-EGFR observed with afatinib treatment (Figs. 4A and 4B).

Digital Autoradiography and Immunohistochemistry

Autoradiographic determination of ^{89}Zr-trastuzumab distribution in afatinib-treated tumors revealed uptake primarily in peripheral tumor regions containing vascularized capsular and stromal tissues. In contrast, localization of ^{89}Zr-trastuzumab in the vehicle-treated control tumors was seen in regions comprising mainly tumor cells (Fig. 5A). A look at the histology of treated and untreated tumor sections displayed decreased staining of afatinib-treated tumors, compared with that of control tumors (Fig. 5B). This distribution pattern was consistent with the imaging data in Figure 3B, where a reduction in HER2 expression after afatinib treatment was accompanied by a reduction in ^{89}Zr-trastuzumab binding. Immunohistochemical examination of tumor sections for the proliferation marker Ki-67 (Supplemental Fig. 5) revealed reduction in the number of proliferating tumor cells after afatinib, whereas the apoptosis marker cleaved caspase 3 revealed no significant

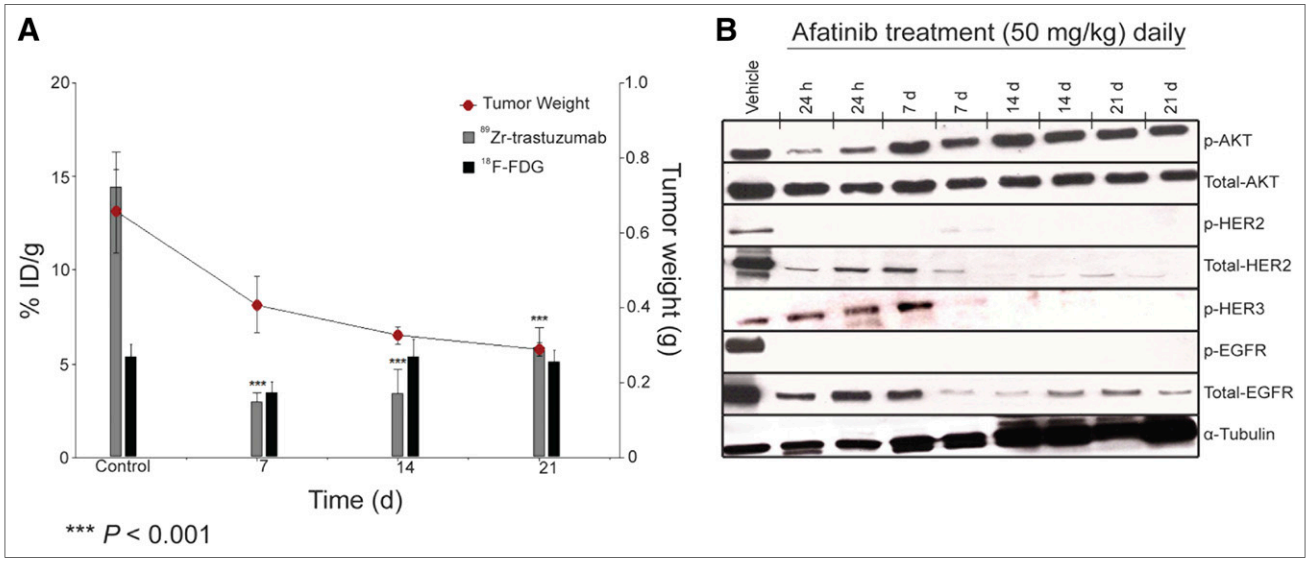

FIGURE 4. Correlative analysis between ^{89}Zr-trastuzumab and ^{18}F-FDG tumor uptake with tumor weight and HER2 levels. (A) Bar charts show ROIs (%ID/g) for ^{89}Zr-trastuzumab and ^{18}F-FDG uptake in NCI-N87 tumors recorded and superimposed with tumor weight (graph) at baseline, 7 d, 14 d, and 21 d after treatment with afatinib (50 mg/kg daily). (B) Western blot analyses of tumors harvested from HER2-positive NCI-N87 xenografts treated with vehicle or afatinib (50 mg/kg orally daily); specimen collected at 1, 7, 14, and 21 d after treatment.

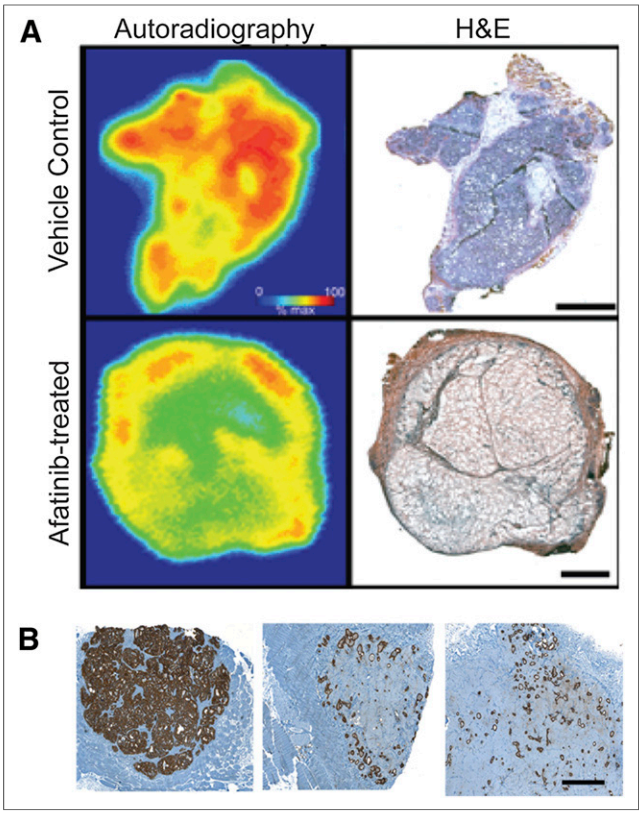

FIGURE 5. Autoradiographic determination of ^{89}Zr-trastuzumab distribution and HER2 histology of HER2-positive xenografts. (A) Frozen sections (10 μm) from NCI-N87 xenografts treated with afatinib (50 mg/kg) or vehicle for 7 d and removed 24 h after administration of ^{89}Zr-trastuzumab. Bar = 2 mm. (B) Representative HER2 immunostaining (brown) of FFPE NCI-N87 tumor sections demonstrating downregulation of HER2 in tumors administered with afatinib (50 mg/kg) at 7 d (middle) and 21 d (right) after treatment, compared with placebo-dosed tumors (left). Bar = 1 mm. H&E = hematoxylin and eosin.

differences between treated and control samples (data not shown). These data suggest that afatinib-mediated reduction in tumor growth observed in these tumor models could be attributed to the inhibition of cellular proliferation rather than direct cytotoxicity. Interestingly, the recovery of ^{89}Zr-trastuzumab tumor–associated uptake and HER2 expression seen after 14 and 21 d of afatinib treatment appears to correspond with increasing Ki-67 staining seen in these tumors and implies a link between HER2 expression and proliferative status, which could be visualized using ^{89}Zr-trastuzumab.

DISCUSSION

In phase II clinical trials evaluating antitumor activity of a chemotherapeutic, drug dose is usually based on toxicity and the maximum tolerated dose determined in phase I studies. Although this approach applies to cytotoxic chemotherapy, it is not ideal for molecularly targeted agents tailored to specific target engagement and inhibition (*28*). Pre- and posttreatment tumor biopsies are now increasingly collected in clinical trials for biomarker development and to characterize the effects of targeted drugs on a molecular level, but these provide only static information on the status of a marker in a small part of the tumor and disregard the heterogeneity within remaining tumor tissue and metastases (*29*).

In HER2-positive esophagogastric cancer, the heterogeneity of HER2 expression within primary tumors and metastasis is a particular challenge (*3*). Moreover, organ distribution of HER2-targeted agents (e.g., trastuzumab) varies in each patient and is heavily affected by the tumor load, which may contribute to variation in patient responses (*30,31*). We need a pharmacodynamic biomarker that can noninvasively assess target engagement and reflect functional effects of targeted agents in the entire tumor and all metastases in patients over time.

Assessment of pharmacodynamic effects of chemotherapeutics with PET imaging using probes specific to the target is a promising method for accomplishing this objective and may ultimately permit dynamic, patient-specific adjustment of drug dosing. Moreover, a decrease in tumor uptake on PET with treatment may indicate a therapeutic effect at the earliest time point before changes in tumor size appear on CT and will ultimately serve as a predictive biomarker determining which patients are the ones likely to benefit from a particular treatment.

Others have demonstrated that vascular endothelial growth factor PET imaging with ^{89}Zr-ranibizumab allows for serial analysis of angiogenic changes in different areas within a tumor (*32*). The first-in-human ^{89}Zr-trastuzumab HER2 PET imaging showed excellent visualization and quantification of uptake in HER2-positive tumors (*33*). Previously, we demonstrated that ^{89}Zr-trastuzumab PET is highly tumor-specific and can be used to monitor response to treatment with a specific inhibitor of heat-shock protein 90 in breast cancer (*20*). Building on this work, in the present study we evaluated the specificity of ^{89}Zr-trastuzumab, ^{18}F-FDG, and ^{18}F-FLT PET for HER2-positive gastric cancer. Our data demonstrate high tumor uptake of ^{89}Zr-trastuzumab in HER2-positive gastric tumors and minimal nonspecific uptake in HER2-negative tumors, whereas HER2-positive and HER2-negative gastric tumors show equivalent uptake using both ^{18}F-FDG and ^{18}F-FLT PET. PET imaging with ^{89}Zr-trastuzumab PET is highly specific for HER2-positive gastric tumors, but ^{18}F-FDG and ^{18}F-FLT PET are unable to differentiate HER2-positive from HER2-negative tumors. Although ^{18}F-FLT PET may be clinically useful, it was not performed during afatinib therapy because the present study was focused on the correlative effects of afatinib on the molecular target—HER2.

Our data establish potent antitumor activity of the single-agent tyrosine kinase inhibitor of EGFR/HER2/HER4, afatinib, in HER2-positive gastric cancer xenografts and the utility of ^{89}Zr-trastuzumab PET instead of ^{18}F-FDG PET as a pharmacodynamic marker of HER2 target inhibition in response to afatinib. Although ^{18}F-FDG uptake in HER2-positive gastric

tumors does not change with afatinib therapy, a decrease in ^{89}Zr-trastuzumab uptake was observed in the afatinib-treated group, compared with the control group (3.0 ± 0 %ID/g vs. 21.0 ± 3.4 %ID/g; $P < 0.05$). This change in radiotracer uptake correlated with downregulation of HER2 activity on immunoblots and immunohistochemistry and decreased tumor size. In chronic myelogenous leukemia, the magnitude of breakpoint cluster region–Abelson tyrosine-protein kinase activity inhibition was found to correlate with clinical outcome (*34*), highlighting the utility of a pharmacodynamic marker such as ^{89}Zr-trastuzumab PET in establishing the final registration dose as afatinib enters clinical trials in HER2-positive esophagogastric cancer.

Although ^{18}F-FDG PET has the proven ability to monitor pharmacodynamic changes with tyrosine kinase inhibitor therapy in melanoma with vemurafenib (*35*), gastrointestinal stromal tumors with imatinib (*36*), and lung adenocarcinoma with erlotinib (*37*), we demonstrated that ^{18}F-FDG is not specific for HER2-driven tumors and is unable to monitor pharmacodynamic effects of afatinib in HER2-positive gastric cancer. ^{89}Zr-trastuzumab PET provides specific delineation of HER2-positive gastric cancer. ^{89}Zr-trastuzumab has clinical utility as a pharmacodynamic biomarker of HER2 inhibition by afatinib in HER2-positive gastric cancer and may show value as a predictive biomarker by indicating at 7 d which tumors will shrink and which patients will eventually derive clinical benefit from afatinib therapy. Efforts are ongoing to generate a HER2-positive ^{89}Zr-trastuzumab–avid model refractory to afatinib and to determine that in the drug-insensitive tumor model, ^{89}Zr-trastuzumab does not change with afatinib therapy.

We hypothesize that ^{89}Zr-trastuzumab PET may surpass the ^{18}F-FDG PET–guided treatment algorithm for diagnosis, staging, monitoring of treatment response, and personalized selection of drug dose in HER2-positive esophagogastric cancer. An Investigational New Drug application will be submitted to the U.S. Food and Drug Administration for ^{89}Zr-trastuzumab PET for clinical development in HER2-positive gastric cancer patients treated with afatinib in an ongoing phase II study and into the predictive biomarker utility of ^{89}Zr-trastuzumab PET (clinicaltrials.gov; NCT01522768).

CONCLUSION

Here, we have shown that ^{89}Zr-trastuzumab PET, compared with ^{18}F-FDG and ^{18}F-FLT, specifically delineated HER2-positive gastric tumors. Antitumor activity of the small-molecule EGFR/HER2/HER4 inhibitor afatinib has proven more potent than the combination of trastuzumab and afatinib or trastuzumab alone, as supported by immunohistology, Western blot, and tumor size reduction measurements. Furthermore, through PET and biodistribution studies, ^{89}Zr-trastuzumab displayed remarkable potential to noninvasively measure the functional effects of afatinib, affording an early predictor of response within and as early as 7 d of therapy, compared with ^{18}F-FDG. Hence, the utility of ^{89}Zr-trastuzumab is extended beyond plain detection and diagnosis of HER2-positive lesions, affording improved patient care and management.

DISCLOSURE

The costs of publication of this article were defrayed in part by the payment of page charges. Therefore, and solely to indicate this fact, this article is hereby marked "advertisement" in accordance with 18 USC section 1734. This study was supported in part by Geoffrey Beene Cancer Center Grant, Boehringer Ingelheim, Germany, and the Office of Science–U.S. Department of Energy (award DE-SC0002456). This study was presented in part at ASCO Molecular Marker Meeting, Hollywood, Florida (2010), and at the ISRS Meeting, Amsterdam, Netherlands (2011). No other potential conflict of interest relevant to this article was reported.

REFERENCES

1. Bang YJ, Van Cutsem E, Feyereislova A, et al. Trastuzumab in combination with chemotherapy versus chemotherapy alone for treatment of HER2-positive advanced gastric or gastro-oesophageal junction cancer (ToGA): a phase 3, open-label, randomised controlled trial. *Lancet.* 2010;376:687–697.
2. Tafe LJ, Janjigian YY, Zaidinski M, et al. Human epidermal growth factor receptor 2 testing in gastroesophageal cancer: correlation between immunohistochemistry and fluorescence in situ hybridization. *Arch Pathol Lab Med.* 2011;135:1460–1465.
3. Hofmann M, Stoss O, Shi D, et al. Assessment of a Her2 scoring system for gastric cancer: results from a validation study. *Histopathology.* 2008;52:797–805.
4. Bang YJ, Van Cutsem E, Feyereislova A, et al. Trastuzumab in combination with chemotherapy versus chemotherapy alone for treatment of HER2-positive advanced gastric or gastro-oesophageal junction cancer (ToGA): a phase 3, open-label, randomised controlled trial. *Lancet.* 2010;376:687–697.
5. Yarden Y, Sliwkowski MX. Untangling the ErbB signalling network. *Nat Rev Mol Cell Biol.* 2001;2:127–137.
6. Yang JC, Shih JY, Su WC, et al. Afatinib for patients with lung adenocarcinoma and epidermal growth factor receptor mutations (LUX-Lung 2): a phase 2 trial. *Lancet Oncol.* 2012;13:539–548.
7. Agulnik M. New approaches to EGFR inhibition for locally advanced or metastatic squamous cell carcinoma of the head and neck (SCCHN). *Med Oncol.* 2012;29:2481–2491.
8. Brugger W, Thomas M. EGFR-TKI resistant non-small cell lung cancer (NSCLC): new developments and implications for future treatment. *Lung Cancer.* 2012;77:2–8.
9. Schuler M, Awada A, Harter P, et al. A phase II trial to assess efficacy and safety of afatinib in extensively pretreated patients with HER2-negative metastatic breast cancer. *Breast Cancer Res Treat.* 2012;134:1149–1159.
10. De Grève J, Teugels E, Geers C, et al. Clinical activity of afatinib (BIBW 2992) in patients with lung adenocarcinoma with mutations in the kinase domain of HER2/neu. *Lung Cancer.* 2012;76:123–127.
11. Hickish T, Wheatley D, Lin N, et al. Use of BIBW 2992, a novel irreversible EGFR/HER1 and her2 tyrosine kinase inhibitor to treat patients with HER2-positive metastatic breast cancer after failure of treatment with trastuzumab. *Cancer Res.* 2009;69(24 suppl):5060.
12. Lordick F, Ott K, Krause BJ, et al. PET to assess early metabolic response and to guide treatment of adenocarcinoma of the oesophagogastric junction: the MUNICON phase II trial. *Lancet Oncol.* 2007;8:797–805.
13. Weber WA, Ott K, Becker K, et al. Prediction of response to preoperative chemotherapy in adenocarcinomas of the esophagogastric junction by metabolic imaging. *J Clin Oncol.* 2001;19:3058–3065.
14. Ott K, Weber WA, Lordick F, et al. Metabolic imaging predicts response, survival, and recurrence in adenocarcinomas of the esophagogastric junction. *J Clin Oncol.* 2006;24:4692–4698.
15. Stahl A, Ott K, Weber WA, et al. FDG PET imaging of locally advanced gastric carcinomas: correlation with endoscopic and histopathological findings. *Eur J Nucl Med Mol Imaging.* 2003;30:288–295.
16. Smith-Jones PM, Solit DB, Akhurst T, Afroze F, Rosen N, Larson SM. Imaging the pharmacodynamics of HER2 degradation in response to Hsp90 inhibitors. *Nat Biotechnol.* 2004;22:701–706.

17. Niu G, Li Z, Cao Q, Chen X. Monitoring therapeutic response of human ovarian cancer with 17-DMAG by noninvasive PET imaging with ^{64}Cu-DOTA-trastuzumab. *Eur J Nucl Med Mol Imaging.* 2009;36:1510–1519.
18. Smith-Jones PM, Solit D, Afroze F, Rosen N, Larson SM. Early tumor response to Hsp90 therapy using HER2 PET: comparison with ^{18}F-FDG PET. *J Nucl Med.* 2006;47:793–796.
19. Holland JP, Sheh Y, Lewis JS. Standardized methods for the production of high specific-activity zirconium-89. *Nucl Med Biol.* 2009;36:729–739.
20. Holland JP, Caldas-Lopes E, Divilov V, et al. Measuring the pharmacodynamic effects of a novel Hsp90 inhibitor on HER2 expression in mice using Zr-DFO-trastuzumab. *PLoS ONE.* 2010;5:e8859.
21. Holland JP, Divilov V, Bander NH, Smith-Jones PM, Larson SM, Lewis JS. ^{89}Zr-DFO-J591 for immunoPET of prostate-specific membrane antigen expression *in vivo*. *J Nucl Med.* 2010;51:1293–1300.
22. Anderson CJ, Connett JM, Schwarz SW, et al. Copper-64-labeled antibodies for PET imaging. *J Nucl Med.* 1992;33:1685–1691.
23. Anderson CJ, Schwarz SW, Connett JM, et al. Preparation, biodistribution and dosimetry of copper-64-labeled anti-colorectal carcinoma monoclonal antibody fragments 1A3-F(ab')2. *J Nucl Med.* 1995;36:850–858.
24. Lindmo T, Bunn PA Jr. Determination of the true immunoreactive fraction of monoclonal antibodies after radiolabeling. *Methods Enzymol.* 1986;121:678–691.
25. Carlin S, Khan N, Ku T, Longo VA, Larson SM, Smith-Jones PM. Molecular targeting of carbonic anhydrase IX in mice with hypoxic HT29 colorectal tumor xenografts. *PLoS ONE.* 2010;5:e10857.
26. Regales L, Gong Y, Shen R, et al. Dual targeting of EGFR can overcome a major drug resistance mutation in mouse models of EGFR mutant lung cancer. *J Clin Invest.* 2009;119:3000–3010.
27. Heneweer C, Holland JP, Divilov V, Carlin S, Lewis JS. Magnitude of enhanced permeability and retention effect in tumors with different phenotypes: ^{89}Zr-albumin as a model system. *J Nucl Med.* 2011;52:625–633.
28. Sawyers CL. The cancer biomarker problem. *Nature.* 2008;452:548–552.
29. de Vries EGE, Munnink THO, van Vugt MATM, Nagengast WB. Toward molecular imaging–driven drug development in oncology. *Cancer Discov.* 2011;1:25–28.
30. Leyland-Jones B, Colomer R, Trudeau ME, et al. Intensive loading dose of trastuzumab achieves higher-than-steady-state serum concentrations and is well tolerated. *J Clin Oncol.* 2010;28:960–966.
31. Oude Munnink TH, Dijkers EC, Netters SJ, et al. Trastuzumab pharmacokinetics influenced by extent human epidermal growth factor receptor 2-positive tumor load. *J Clin Oncol.* 2010;28:e355–356.
32. Nagengast WB, Lub-de Hooge MN, Oosting SF, et al. VEGF-PET imaging is a noninvasive biomarker showing differential changes in the tumor during sunitinib treatment. *Cancer Res.* 2011;71:143–153.
33. Dijkers EC, Oude Munnink TH, Kosterink JG, et al. Biodistribution of ^{89}Zr-trastuzumab and PET imaging of HER2-positive lesions in patients with metastatic breast cancer. *Clin Pharmacol Ther.* 2010;87:586–592.
34. Shah NP, Kantarjian HM, Kim DW, et al. Intermittent target inhibition with dasatinib 100 mg once daily preserves efficacy and improves tolerability in imatinib-resistant and -intolerant chronic-phase chronic myeloid leukemia. *J Clin Oncol.* 2008;26:3204–3212.
35. McArthur GA, Puzanov I, Amaravadi R, et al. Marked, homogeneous, and early [18f]fluorodeoxyglucose-positron emission tomography responses to vemurafenib in BRAF-mutant advanced melanoma. *J Clin Oncol.* 2012;30:1628–1634.
36. Gayed I, Vu T, Iyer R, et al. The role of ^{18}F-FDG PET in staging and early prediction of response to therapy of recurrent gastrointestinal stromal tumors. *J Nucl Med.* 2004;45:17–21.
37. Benz MR, Herrmann K, Walter F, et al. ^{18}F-FDG PET/CT for monitoring treatment responses to the epidermal growth factor receptor inhibitor erlotinib. *J Nucl Med.* 2011;52:1684–1689.

JNM The Journal of NUCLEAR MEDICINE

Monitoring Afatinib Treatment in HER2-Positive Gastric Cancer with ^{18}F-FDG and ^{89}Zr-Trastuzumab PET

Yelena Y. Janjigian, Nerissa Viola-Villegas, Jason P. Holland, Vadim Divilov, Sean D. Carlin, Erica M. Gomes-DaGama, Gabriela Chiosis, Gregory Carbonetti, Elisa de Stanchina and Jason S. Lewis

J Nucl Med. 2013;54:936-943.
Published online: April 11, 2013.
Doi: 10.2967/jnumed.112.110239

The Journal of Nuclear Medicine is published monthly.
SNMMI | Society of Nuclear Medicine and Molecular Imaging
1850 Samuel Morse Drive, Reston, VA 20190.
(Print ISSN: 0161-5505, Online ISSN: 2159-662X)

SNMMI SOCIETY OF NUCLEAR MEDICINE AND MOLECULAR IMAGING